AIP | Journal of Applied Physics

Memory effects in superparamagnetic and nanocrystalline Fe50Ni50 alloy

D. De, A. Karmakar, M. K. Bhunia, A. Bhaumik, S. Majumdar, and S. Giri

Citation: Journal of Applied Physics **111**, 033919 (2012); doi: 10.1063/1.3684624
View online: http://dx.doi.org/10.1063/1.3684624
View Table of Contents: http://scitation.aip.org/content/aip/journal/jap/111/3?ver=pdfcov
Published by the AIP Publishing

Memory effects in superparamagnetic and nanocrystalline $Fe_{50}Ni_{50}$ alloy

D. De,[1,2] A. Karmakar,[1] M. K. Bhunia,[3] A. Bhaumik,[3] S. Majumdar,[1] and S. Giri[1,a)]
[1]*Department of Solid State Physics, Indian Association for the Cultivation of Science, Jadavpur, Kolkata 700032, India*
[2]*ITME, Diamond Harbour Road, 24 PGS (S), West Bengal, India*
[3]*Department of Materials Science, Indian Association for the Cultivation of Science, Jadavpur, Kolkata 700032, India*

(Received 22 September 2011; accepted 11 January 2012; published online 14 February 2012)

Nanocrystalline $Fe_{50}Ni_{50}$ alloy is prepared using the sol-gel route in an amorphous silica host at different volume fractions (ϕ). The average particle size is 8.9 nm having log-normal distribution = 0.19, which is confirmed by transmission electron microscopy for $\phi = 1\%$. The blocking temperature (T_B) is 30 K, as observed in dc magnetization. The frequency-dependent peak-shift in ac susceptibility satisfies Néel-Arrhenius formalism with more reasonable physical parameters than Vogel-Fulcher and dynamical scaling formalisms. Analysis of the relaxation dynamics below T_B points toward weak interparticle interaction, signifying superparamagnetic behavior. Relaxation dynamics following stretched exponential function implies that it is involved with the activation against multiple anisotropy barriers, which is correlated to the distribution of particle size. Memory effects are observed in different experimental protocols below T_B, which has been discussed pertaining to superparamagnetic behavior. © *2012 American Institute of Physics*. [doi:10.1063/1.3684624]

I. INTRODUCTION

The assembly of magnetic nanoparticles is well recognized for promising technological applications in different aspects, such as magnetic recording media, spin-electronic devices, ferrofluids, biosensors, drug delivery in biology, etc. Pure metal has a saturation magnetization approximately four times than that of its oxide, which motivates us to use metal particles, where coercivity of the material commensurates with their higher moment for different applications. Unfortunately, small particles of pure metal have a strong tendency of oxidation and their stabilization can be accomplished typically through alloying and/or the controlled oxidation on the surface. Therefore, the problem of stabilization of metal particles from its oxidation is one of the motivations for intense research on ultrafine nanoparticles of metal alloys. Binary alloys of Ni are significant in this respect because of their inertness to the oxidation. Since the discovery of the Invar effect in fcc Ni-Fe alloys,[1] this type of alloy has drawn considerable attention for fundamental interests and promising technological applications.[2,3] For the range of Ni from 35% to 90%, Ni-Fe magnetic alloys are termed as permalloy, which are probably the most versatile soft magnetic alloys being used today. Permalloy has a high magnetic permeability, low coercivity, very small magnetostriction, and significant anisotropic magnetoresistance. These types of fascinating properties have useful technological applications in transformer, laminations, magnetic screening, magnetic amplifier, and magnetic recording head sensors.[4] Although compared to bulk counterpart, less investigation is done on nanocrystalline alloys, these have been revisited on and off because of its tremendous technological applications. A quick survey of the literature proves the diversity of research in such a related alloy system.

Injection-molded FeNi-sintered bodies were fabricated using nano Fe50%Ni powders having an average size of 80 nm.[5] Their microstructures and material properties were investigated at different compositions and sintering temperatures. The bilayer structures of $Fe_{50}Ni_{50}$ films on silicon substrates have been investigated in the recent past.[6] Magnetization was understood in the realm of interfacial intermixing, leading to nano-granular phases of magnetic silicides. Diluted nanoparticles of $Co_{80}Fe_{20}/Al_2O_3$ multilayer systems are also being studied adequately, where tuning of interparticle interactions can control transition from a superparamagnetic (SPM) to a superferromagnetic (SFM) state through an intermediate superspin-glass (SSG) state.[7–12]

An ensemble of nanoparticles may display superparamagnetic behavior when interparticle interaction is negligible. This state is well described by the Néel-Arrhenius model, which deals with magnetic anisotropy of an individual particle. When interparticle interaction is not negligible, individual anisotropic property no longer exists and a collective behavior appears. With an increase of interparticle interaction, at an intermediate stage, the particle as a whole shows an atomic spin-glass (SG)-like behavior, which is termed as superspin-glass state.[13] In the study of magnetic nanoparticles, the term *super* is very commonly used, because very large moment $(10^2 \sim 10^4)\mu_B$, having a single domain structure and uniaxial anisotropy, is typically observed compared to a few μ_B moments, like in atomic SG. At sufficiently strong interaction below the percolation threshold, a superferromagnetic state can be realized in practice.[13]

In this study, we investigate chemically synthesized nanocrystalline $Fe_{50}Ni_{50}$ particles embedded in an amorphous silica matrix having volume fractions (ϕ) of 1%, 5%, and 10%.

a)Electronic mail: sspsg2@iacs.res.in.

Detailed investigations are carried out at $\phi = 1\%$. The dynamics of dc magnetization and frequency dependence of ac susceptibility point toward superparamagnetic behavior of weakly interacting nanoparticles. Interesting memory effects in different experimental protocols of time and thermal variation of magnetization are observed in this nanocrystalline alloy. The issue of the memory effect is discussed in connection to superparamagnetism.

II. EXPERIMENT

A nanocrystalline alloy with composition $Fe_{50}Ni_{50}$ embedded in a SiO_2 matrix was prepared by standard sol-gel technique with ϕ of 1%, 5%, and 10%.[14] Pure Fe and Ni powders were dissolved in nitric acid (70% diluted) separately. Citric acid was added to the stoichiometrically mixed solution of metal nitrates and homogenized thoroughly. The solution was transparent with a greenish tinge. Ethanolic tetraethyl orthosilicate (TEOS) was finally added to the solution in the form of droplets and mixed thoroughly for 12 h to obtain homogeneous mixture. TEOS was used as a source of SiO_2 matrix. The resulting greenish and transparent solution was dried very slowly to form a gel at room temperature for 15 days. The dried gel was decomposed at 600 °C for 6 h in a continuous flow of H_2/argon mixture (5% H_2 and 95% argon). We consider the molar ratios of Fe/Ni/TEOS = 1/1/5, 1/1/11, and 1/1/58 for obtaining final products of an $Fe_{50}Ni_{50}$ alloy with ϕ of 10%, 5%, and 1%, respectively.

The actual composition was confirmed by transmission electron microscopy (TEM) equipped with an energy dispersive x ray spectrometer (JEOL TEM, 2010). Sizes of the particles were confirmed by TEM. Powder x ray diffraction (XRD) studies were performed in a diffractometer (Seifert XRD 3000P) with the Cu Kα radiation source. dc magnetization and ac susceptibility measurements were carried out in a commercial superconducting quantum interference device (SQUID) magnetometer of Quantum Design (MPMS, XL). In the case of zero-field cooled (ZFC) protocol, the sample was cooled down to low temperature in zero-field and magnetization was measured in warming mode with a static magnetic field. Magnetic field was applied during cooling of the sample in the field-cooled (FC) mode, and measurement was performed in the warming cycle like a ZFC measurement.

III. RESULTS AND DISCUSSIONS

A. Structural properties

The XRD patterns of $Fe_{50}Ni_{50}$ at $\phi = 1\%$, 5%, and 10% are shown in Fig. 1(a), which could be fitted in face-centered cubic structure ($Fm3m$) with $a = 3.56$ Å. All the diffraction peaks are indexed, which is shown in the figure. The electron diffraction (ED) pattern is in accordance with the XRD pattern, where rings corresponding to different planes are highlighted in Fig. 1(d) for $\phi = 1\%$.[5] The results obtained from two different techniques confirm the absence of secondary crystalline phases. Grain size and morphology of particles are investigated for $\phi = 1\%$ and 5% using TEM. The TEM image for $\phi = 1\%$ is displayed in Fig. 1(b). Since the volume fraction is low for $\phi = 1\%$, it is difficult to find a large number of particles in an image to obtain a histogram of size distribution. So several drops were added on the grid, which results in several overlapped layers on the TEM grid. This is noticeable from the wide variation of intensities of particle images in the TEM picture. The inset of Fig. 1(b) exhibits a histogram of particle size. Particle size distribution is fitted with log-normal distribution function with an average size = 8.9 nm and log-normal distribution function = 0.19.

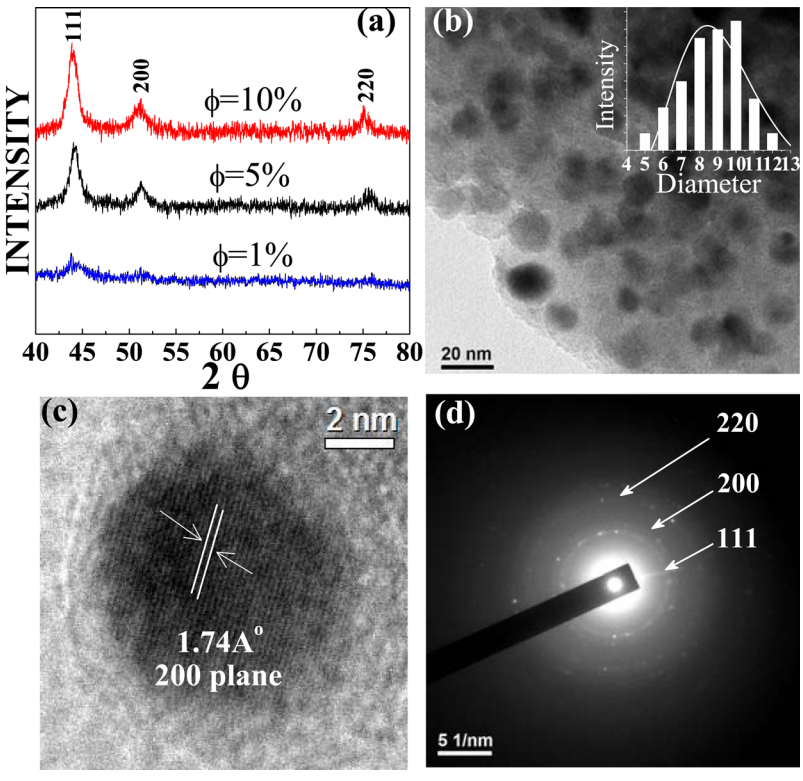

FIG. 1. (Color online) (a) X ray diffraction patterns of nanocrystalline $Fe_{50}Ni_{50}$ for $\phi = 1\%$, 5%, and 10%. (b) TEM image of $Fe_{50}Ni_{50}$ for $\phi = 1\%$. Inset shows histogram of particle size. Continuous curve displays fit using log-normal distribution function. (c) High-resolution TEM image of a particle. (d) ED patterns for $\phi = 1\%$.

Particles are nearly spherical and diameter varies from 5 nm to 12 nm. We note that the shape of the particles for $\phi = 5\%$ are identical, although a larger size and distribution are observed in between 8.0-20.0 nm. A high-resolution TEM image of a particle for $\phi = 1\%$ is shown in Fig. 1(c), which clearly demonstrates good crystallinity, even close to the edge of the particle. This is the key factor for proper understanding of magnetic and electronic properties of nanoparticles.[15] As highlighted in Fig. 1(c), the minimum distance between planes is found to be close to that obtained from XRD analysis (1.78 Å corresponding to (200) with lattice constant, $a = 3.56$ Å).

B. dc magnetization

Detailed magnetic investigation is performed on nanocrystalline $Fe_{50}Ni_{50}$ of ϕ at 1% and 5%. Thermal variation of FC-ZFC magnetization measured at 100 Oe is shown in Fig. 2(a). A broadened maximum (T_M) around 255 K is noticeable for $\phi = 5\%$. The inset of Fig. 2(a) magnifies the position of the maximum. It is to be noted that FC magnetization of $\phi = 5\%$ does not meet with ZFC magnetization, even at close to room temperature (300 K). This may indicate that the bifurcation temperature is much higher than T_M. The result may be correlated to a large distribution of particle size, as seen in the TEM image. On the other hand, a well-defined peak is observed at $T_B = 30$ K in ZFC magnetization for $\phi = 1\%$. FC magnetization exhibits a steep increasing trend with decreasing temperature below T_B. This primarily indicates the superparamagnetic blocking process below T_B. Magnetic hysteresis loops are measured at 4 K for both the samples. Hysteresis loops with moderate coercivity and remanence are observed for both the samples [shown in Fig. 2(b)]. As seen in the inset of Fig. 2(b), magnetisation of $\phi = 1\%$ does not saturate at 50 kOe, whereas a clear signature of saturation of magnetization is observed for $\phi = 5\%$. The value of saturation magnetization is $\approx 1.2\ \mu_B$, which is close, but still lower than the average moment (1.4 μ_B) of bulk Fe and Ni.[16] The coercivity ($H_C \approx 0.5$ kOe) is larger for $\phi = 1\%$ than that of the value ($H_C \approx 0.3$ kOe) for $\phi = 5\%$. In the case of superparamagnetic nanoparticles, coercivity and remanence magnetization should not appear. Practically, small values of coercivity and remanence usually appear due to extrinsic effects, such as disorders, discontinuity in coordination numbers, and defects at the grain boundary, as found in the literature.[37–40] These extrinsic effects at the grain boundary are usually referred to as surface effect. In the current investigation, moderate values of coercivity and remanence appearing for $\phi = 1\%$ are correlated to mainly surface effect. We note that larger coercivity is associated with dominant surface effect at $\phi = 1\%$, in which average particle size is much smaller than the particles with $\phi = 5\%$. This indicates that extrinsic surface effect leads to the appearance of coercivity and remanence for proposed superparamagnetic nanoparticles.

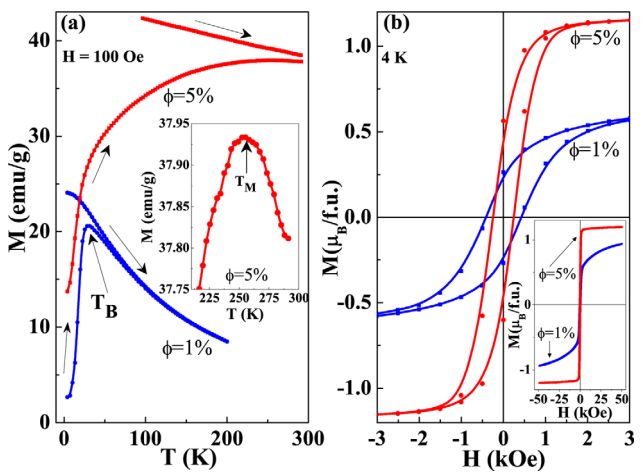

FIG. 2. (Color online) (a) Temperature variation of ZFC and FC magnetizations for $\phi = 1\%$ and 5% measured at 100 Oe. Inset magnifies the maximum in ZFC curve for $\phi = 5\%$. (b) Magnified $M - H$ loop for $\phi = 1\%$ and 5%. Inset shows $M - H$ loop in between ± 50 kOe.

C. ac susceptibility

The ac susceptibility (χ_{ac}) was measured around the peak observed in ZFC magnetization at five different frequencies (f) in the range of 1–444 Hz with ac field, $H_{ac} = 3$ Oe, for $\phi = 1\%$. The thermal variation of real, $\chi'(T)$, and imaginary part, $\chi''(T)$, of χ_{ac} are displayed in Figs. 3(a) and 3(b), respectively. The maximum (T_p) in $\chi'(T)$ is shifted considerably toward a higher temperature with increase in f. The value of $\Delta T_p = 8.25$ K for change in f from 1 to 444 Hz. This f-shift in T_p primarily distinguishes the nanoparticles from atomic SG systems. It may be noted that values of $\Delta T_p/[T_p \Delta(\log\ \omega)]$ lie in the range 0.005–0.010 for metallic SG and 0.06-0.08 for insulating SG compounds, where $\omega = 2\pi f$. Typically, non-interacting SPM

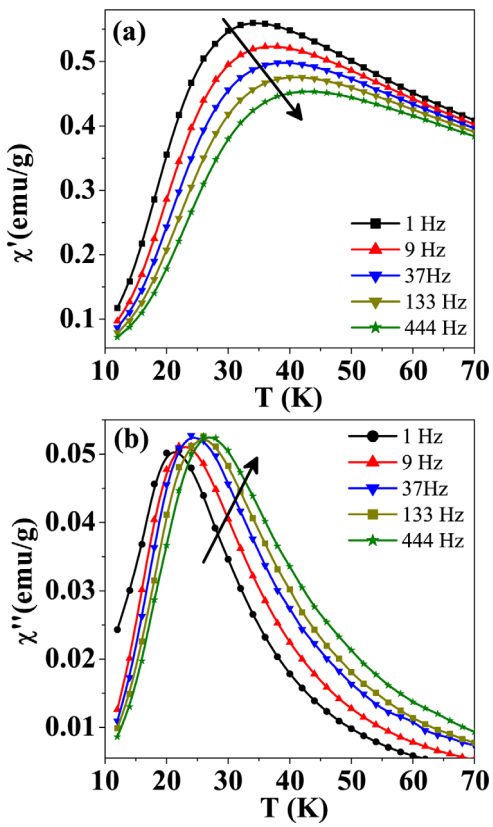

FIG. 3. (Color online) Thermal variation of real part, $\chi'(T)$, and imaginary part, $\chi''(T)$, of χ_{ac} at different f for $\phi = 1\%$. The arrows indicate direction of increasing f.

nanoparticles show comparatively larger value of $\Delta T_p/[T_p\Delta(\log \omega)] \approx 0.1$. In the current investigation, the value of $\Delta T_p/[T_p\Delta(\log \omega)] = 0.07$ for $\phi = 1\%$, indicating the SPM nature of the nanoparticles.

In an assembly of noninteracting SPM nanoparticles, relaxation time (τ) follows Néel-Arrhenius law defined as

$$\tau = \tau_0 \exp(E_a/k_B T_p), \quad (1)$$

where E_a is the anisotropy energy of an individual particle and τ is the inverse of measuring frequency ($1/2\pi f$). τ_0 is the attempt time, which is typically found in the range of 10^{-13}-10^{-15} s for SPM nanoparticles. The linear plot of $1/T_p$ with $\ln f$ for $\chi'(T)$ is shown in Fig. 4(a). Linear fit using Eq. (1) provides $\tau_0 = 10^{-15}$ s, which is well within the range observed for SPM nanoparticles. The value of E_a/k_B is found to be 1109 K for $\chi'(T)$, which is reasonable compared to the value of $KV/k_B = T_p \ln(t/\tau_0) = 1312$ K, considering typical values of $t = 100$ s and $\tau_0 = 10^{-13}$ s. In the case of interacting particles, the f-dependent T_p follows the Vogel-Fulcher law described as

$$\tau = \tau_0 \exp[(E_a/k_B(T_p - T_{VF})], \quad (2)$$

where T_{VF} brings in interaction between the particles, which provides modified values of E_a/k_B and τ_0. The plot of T_p versus $\ln f$ satisfying Vogel-Fulcher formalism is displayed in Fig. 4(a). The values of T_{VF}, E_a/k_B, and τ_0 obtained from the fit are 12.6 K, 502.3 K, and $\sim 10^{-11}$ s, respectively, from $\chi'(T)$. The value of T_{VF} is much lower than the T_B obtained from dc magnetization, and τ_0 is much faster than the value ($\sim 10^{-9}$ s) for atomic SG. Analysis of f-dependent $\chi'(T)$ clearly demonstrates that Néel-Arrhenius formalism provides a more physical set of parameters than the fit using Vogel-Fulcher law.

The other approach of analyzing f-dependence of $\chi'(T)$ is the standard theory of dynamical scaling near the phase transition at T_p, which relates the critical relaxation time, τ_{max}, to the correlation length, ζ, as

$$\tau_{max} = \tau_0' \zeta^{z\nu}, \quad (3)$$

where $\zeta = T_0/(T_p - T_0)$, τ_0' is the microscopic flipping time, z is the dynamic exponent, ν is the spin-correlation length exponent, and T_0 provides the dc value of T_p for $\omega \to 0$. The best fit for $\chi'(T)$ is shown in Fig. 4(b). The value of T_0 obtained is 25.6, which is much lower than $T_B = 30$ K obtained from dc magnetization. The value of $z\nu$ is 9.6, which holds good in the range between 4 and 12 typically found for atomic SG compounds. Moreover, τ_0' is $\sim 10^{-6}$ s, which is much slower than the values in the range, $\sim 10^{-12}$–10^{-14} for atomic SG compounds.[17]

D. Relaxation dynamics

Time (t) dependence of dc magnetization (M) was measured for the sample of $\phi = 1\%$. The sample was cooled down to 15 K (well below T_B) from room temperature in the applied field 50 Oe, and magnetization was recorded with t in zero-field after stabilizing the temperature at 15 K. In Fig. 5(a), the t dependence of M at 15 K is plotted, which is fitted with the stretched exponential function,

$$M(t) = M_0 - M_g \exp(-t/\tau^{\beta}), \quad (4)$$

where M_0 and M_g are the ferromagnetic (FM) and exponential components of magnetization. β is an exponent which lies in the range $0 < \beta \leq 1$. In the above expression, $\beta = 1$ indicates that the relaxation mechanism involves activation against a single anisotropy barrier, whereas $\beta < 1$ indicates activation against multiple anisotropy barriers. It may be noted that M_0 was required to fit the low-t region of the $M - t$ curve. Satisfactory linear fit is displayed in Fig. 5(a) in a plot of $\ln[M(t) - M_0]$ with t^{β}, using Eq. (4). The values of M_0, M_g, τ, and β are 3.61 emu/g, –2.20 emu/g, 2185.3 s, and 0.45, respectively. A significantly large value of M_0 indicates the signature of the dominant FM component in the relaxation dynamics, as found in a nanocrystalline CoNi alloy.[14] We note that f dependence

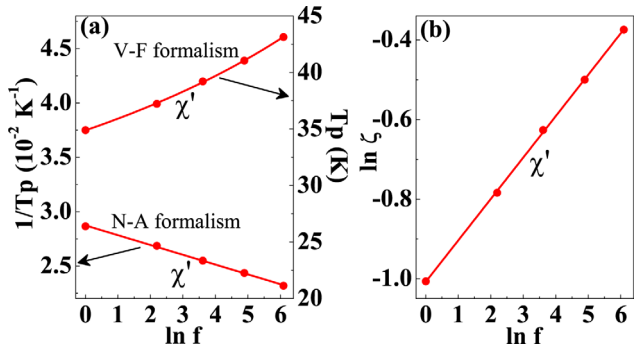

FIG. 4. (Color online) (a) Plot of $1/T_p$ with $\ln f$ according to Néel-Arrhenius (N-A) formalism and plot of T_p against $\ln f$ satisfying Vogel-Fulcher (V-F) formalism for $\chi'(T)$. (b) Plot of $\ln \zeta$ against $\ln f$ according to dynamical scaling approach for $\chi'(T)$.

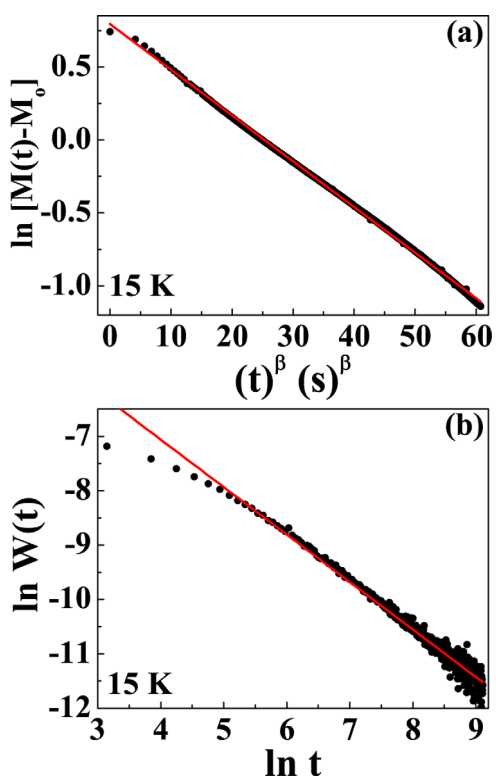

FIG. 5. (Color online) (a) Linear plot of $\ln[M(t) - M_0]$ vs t^{β} at 15 K, where t is given in s. Solid straight line shows the fit using stretched exponential function. (b) Time (t) dependence of $W(t)$ at 15 K, where t is given in s. Solid straight line exhibits the fit using Eq. (5).

of $\chi'(T)$ satisfies Néel-Arrhenius formalism, typically found for superparamagnetic nanoparticles. The value of $\beta = 0.45$ obtained from the fit clearly points to the activation against multiple anisotropy barriers. Here, the existence of multiple anisotropy barriers possibly bears correlation to the signature of the distribution of the particle size.[18]

Recently, Ulrich proposed a relaxation mechanism based on Monte Carlo simulation, where dipolar interactions have only been taken into account to interpret slow relaxation processes of ferromagnetic nanoparticles.[19] They explicitly showed that decay of $M(t)$ follows the following relation after the lapse of a crossover time, t_0,

$$W(t) = t^{-n}, \tag{5}$$

where $W(t)$ is defined as $-(d/dt)\ \ln M(t)$. In the above expression, the value of n is crucial, which is ≥ 1 for dense and $\approx 2/3$ for weakly interacting, diluted FM nanoparticles embedded in a nonmagnetic matrix having a distribution in particle size. This theoretical model nicely interprets the relaxation dynamics of magnetic clusters[20,21] and nanoparticles,[22,23] while it has been useful to probe the strength of the interparticle dipole-dipole interaction. The plot of $\ln W(t)$ against $\ln t$ is given in Fig. 5(b). The straight line fit is displayed after $t_0 = 2 \times 10^2$ s and with $n = 0.66$. The value of n is significant, which indicates weak interparticle dipole-dipole interaction for the nanoparticles having volume fraction, $\phi = 1\%$. The result is consistent with that observed in f-dependence of $\chi'(T)$, satisfying Néel-Arrhenius formalism, which is typically considered for non-interacting superparamagnetic nanoparticles.

E. Memory effects

In polydispersive, weakly interacting, or noninteracting nanoparticle systems, a simple model based on lognormal distribution of particle size, giving rise to the distribution of superparamagnetic relaxation time, can interpret the memory effect in the relaxation dynamics.[26] The evidence of memory effects in such nanoparticle systems have been nicely demonstrated in the literature.[18,27,30–32] Examination of memory effects in superparamagnetic and superspin-glass nanoparticles as well as spin-glass systems are carried out through different experimental protocols.[23–25,27–29] Mainly, experimental protocols proposed by Sun *et al.*[25] are performed in the current investigation. Memory effects observed in the relaxation dynamics are summarized in Fig. 6. Figure 6(a) displays isothermal magnetic relaxation at 19 K measured in 100 Oe after zero-field cooling from 120 K, which is well above T_B. Initially, isothermal relaxation was recorded for time, t_1. At the end of t_1, magnetic field was switched off and relaxation was further recorded in zero-field through t_2. Finally, relaxation was again measured for t_3 in 100 Oe. As shown in the inset of Fig. 6(a), relaxation follows single functional dependence when it is plotted for t_1 and t_3 together. The results clearly demonstrate that relaxation retains previous memory of the state, i.e., before temporary switching off the field, when relaxation was again measured in 100 Oe. Figure 6(b) displays magnetic relaxation at 19 K in 100 Oe after zero-field cooling from 120 K. Initially, measurement was carried out for t_1 at 19 K. After, the t_1 sample was cooled to 10 K and relaxation was recorded for t_2. Finally, the sample was heated back to 19 K and relaxation was further recorded for t_3. As seen in the figure, the relaxation process for t_3 is just the continuation of t_1, which is unambiguously depicted in the inset of Fig. 6(b). Similar results are observed at 19 K in the relaxation dynamics measured in zero-field after field-cooling in 100 Oe from 120 K, which is displayed in Fig. 6(c). We note that the relaxation processes described in the insets of Figs. 6(a), 6(b), and 6(c) satisfactorily fit with the stretched exponential function given in Eq. (4). The parameters are listed in Table I. The fitted parameters of the relaxation measured at 19 K and in 100 Oe after ZFC mode exhibit

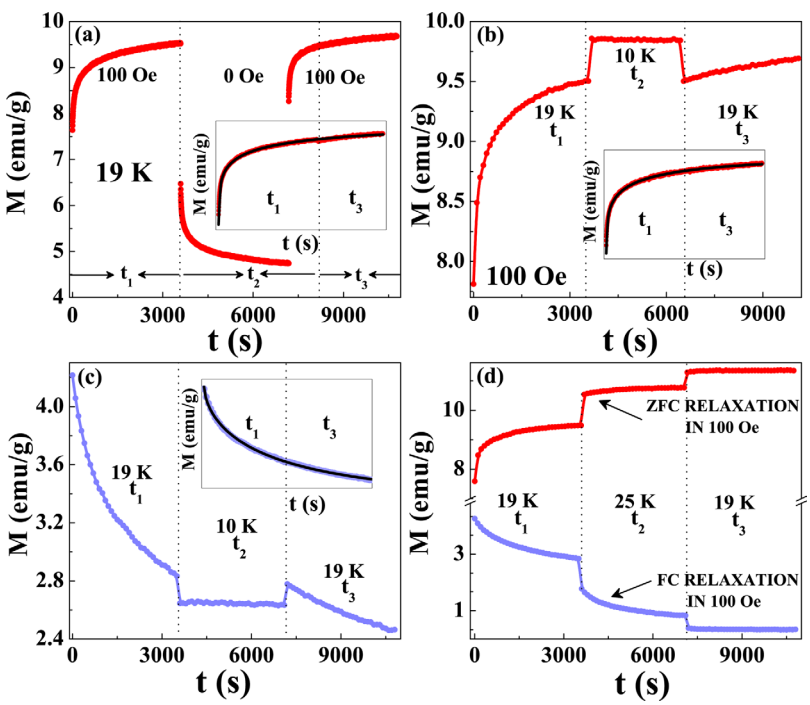

FIG. 6. (Color online) (a) Magnetic relaxation at 19 K and 100 Oe for t_1 and t_3 after cooling in ZFC mode with an intermediate measurement in zero-field for t_2. Inset shows the relaxation in 100 Oe only. (b) Magnetic relaxation at 19 K in zero-field for t_1 and t_3 after FC in 100 Oe with an intermediate cooling at 10 K for t_2. Inset shows the relaxation at 19 K only. (c) Magnetic relaxation at 19 K and 100 Oe for t_1 and t_3 after ZFC with an intermediate cooling at 10 K for t_2. Inset shows relaxation at 19 K only. (d) Magnetic relaxation in zero and 100 Oe after cooling in FC and ZFC modes, respectively, with an intermediate heating at 25 K.

TABLE I. Fitted parameters of time dependence of magnetization measured at different conditions described in the inset of Fig. 6 and at 19 K using Eq. (4).

Parameters	Figure 6(a)	Figure 6(b)	Figure 6(c)
M_0	10.01	9.94	2.07
M_g	2.63	2.31	–2.18
τ	662.0	794.7	3208.9
β	0.31	0.35	0.62

reasonably close values. This indicates that intermediate changes in condition, either by decreasing temperature or by switching field to zero, do not significantly alter the relaxation mechanism. Rather, it repeats the previous history. However, parameters obtained from the fit of relaxation dynamics measured at 19 K and in zero field after cooling in FC mode are considerably different, which is correlated to the measurements in different cooling modes. Overall relaxation results clearly demonstrate that relaxation dynamics before temporary cooling ($T_M - \Delta T$) are exactly retrieved when temperature returns. These are the manifestations of memory effect in the relaxation dynamics. We note that the relaxation process cannot restore previous history when the sample is temporarily heated ($T_M + \Delta T$) instead of cooling, as it is demonstrated in Fig. 6(d) for the measurements in both ZFC and FC. It is noticed that, after returning back to the previous temperature, magnetization does not recall the same level in which it was before the temporary heating. This indicates no memory effect, which is in accordance with those found for interacting nanoparticles[25,33] as well as spin-glass-like GdCu alloy.[34] Current investigation pulls out similar results, even in the case of weakly interacting superparamagnetic nanoparticles.

In the case of the droplet model, *droplet* is defined as the lowest-energy excitation of length scale, **L**.[35] According to this model, the domain grows at a particular temperature and it continues to grow if the domain size is smaller than **L**, even at another temperature. If size becomes larger than **L**, the growth restarts from the state of size **L**. In the case of $T_M - \Delta T$, domain growth proceeds a little, such that it cannot exceed **L**, and the growth process is restored. For example, the change in magnetization during t_2 in the FC relaxation is much smaller ($\sim 0.5\%$) for $T_M - \Delta T$ [see Fig. 6(c)] than the observation ($\sim 50\%$) for $T_M + \Delta T$ [see Figure 6(d)]. The domain size exceeds over **L** for $T_M + \Delta T$, and relaxation initializes fully upon heating. Thus, no memory is observed. This dissimilar response upon heating or cooling is in accordance with the hierarchical model.[36] The absence of memories involved with this temporary heating in the relaxation dynamics is interesting and yet to be extensively investigated experimentally and theoretically on various systems for understanding the underlying mechanism.

Memory effect in the thermal variation of FC magnetization at 100 Oe is investigated, and the results are depicted in Fig. 7(a). At first, magnetization was measured in cooling mode from 120 K down to 4 K with a cooling rate of 1 K/min. During this cooling process, the sample temperature was "halted" or stabilized at two intermediate temperatures at $T_{halt} = 22$ and 12 K for 3 h each. During this halt, the magnetic field was cut off. After completion of each of the 3 h, the magnetic field was reapplied and the measurement was carried on in the same cooling rate down to 4 K. This curve is defined as FC (Waiting), as seen in the figure. Following this, the second cycle of measurement was started in the heating mode at a rate of 1 K/min continuously from 4 K to 120 K, and this curve is designated as the FCH (Memory) curve in the figure. We note comprehensible evidences of steps in the FCH (Memory) curve around T_{halt}, although measurement was carried out continuously without a pause. These steps are the signature of the memory effect [Fig. 7(a)]. For comparison, the FC (Reference) curve defined as a reference field-cooled cooling curve is also displayed in the figure. From repeated experiments, we carefully note that the memory effect is absent in the thermal variation ZFC magnetization curve when the sample was cooled down to 4 K from 120 K without any application of field. This is displayed in the thermal variation of the difference plot (δM) between ZFC (Memory) and ZFC (Reference), as seen in the inset of Fig. 7(b). During the ZFC process, the sample temperature is stabilized at 19 K for 1 h. Any convincing anomaly is not observed at 19 K in the ZFC magnetization plot, which is clearly highlighted in the difference plot, i.e., no memory is imprinted by the aging in zero field. The absence of memory in ZFC mode confirms the superparamagnetic behavior of

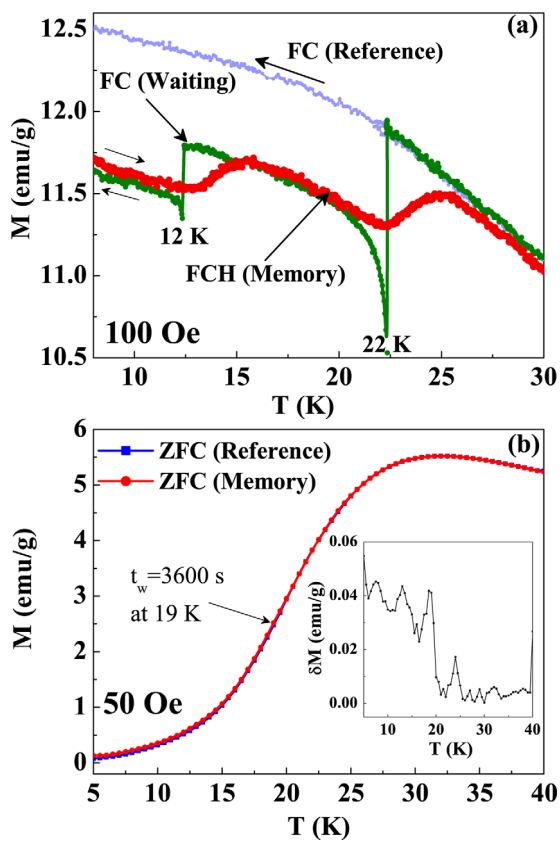

FIG. 7. (Color online) (a) Thermal variation of field-cooled (FC) magnetization in different modes. The field was cutoff during temporary stops at 22 and 12 K. Arrows display the measurements either in cooling or heating modes. Memory effect is demonstrated by the steps close to 22 and 12 K in FCH (Memory) curve. (b) Thermal variation of ZFC magnetization defined as ZFC (Reference) and ZFC magnetization defined as ZFC (Memory) after waiting at 19 K for 3600 s during cooling the sample. Inset shows thermal variation of difference plot (δM) between ZFC (Memory) and ZFC (Reference), displaying absence of convincing signature of memory effect at 19 K.

nanocrystalline $Fe_{50}Ni_{50}$ with ϕ at 1%. This is in accordance with those found for other superparamagnets.[27,32] In superparamagnets, aging and memory effects can originate in FC mode (Fig. 7) and relaxation dynamics (Fig. 6), which appear solely from a broad distribution of relaxation rates. These emerge due to activation against a distribution of energy barriers involving distribution of particle sizes.[26] In a spin-glass, the spin-spin correlation length grows during the stop, even in zero field, and a memory dip typically shows up upon reheating. This is not possible in a noninteracting nanoparticle system and does not show the memory deep in ZFC mode. In noninteracting nanoparticle systems, the distribution of relaxation times originates only from that of the individual particle volumes and is thus an extrinsic effect. On the other hand, it is the consequence of the cooperative phenomenon of spins and is intrinsic and dependent on the age of the system.

IV. CONCLUSION

A single structural phase of a nanocrystalline $Fe_{50}Ni_{50}$ alloy is prepared at different volume fractions. Detailed investigations are performed on the nanocrystalline alloy at 1% volume fraction. Transmission electron microscopy confirms that sizes vary in the range 5-12 nm, with an average size of 8.9 nm. The blocking temperature is observed at 30 K in the ZFC magnetization. Frequency dependence of the peak-shift in ac susceptibility measurements satisfy Néel-Arrheneus formalism, providing reasonable physical parameters than the fits using Vogel-Fulcher and dynamical scaling laws. Analysis of relaxation of magnetization at 15 K (below T_B) points toward weak interparticle interaction, suggesting super-paramagnetic behavior. Relaxation dynamics at 15 K follows stretched exponential function. This implies that relaxation dynamics involves activation against multiple anisotropy barriers and is correlated to the distribution of particle size.

Memory effects are observed in different experimental protocols of thermal variation of FC magnetization and relaxation dynamics below T_B. These are argued to be involved with the distribution of energy barriers, which is ascribed to the particle size distribution of superparamagnetic nanoparticles. Memory effect is absent in the thermal variation of ZFC magnetization, which further confirms noninteracting or weakly interacting super-paramagnetic behavior of nanocrystalline $Fe_{50}Ni_{50}$ alloy having 1% volume fraction.

ACKNOWLEDGMENTS

S.G. wishes to thank Council of Scientific and Industrial Research (Project No. 03(1167)/10/EMR-II), India for the financial support.

SQUID magnetometer of Quantum Design and TEM are used in this study under the DST project, Unit of Nanoscience at Indian Association for the Cultivation of Science, Jadavpur, India.

[1]Ch. Éd. Guillaume, C. R. Hebd. Seances Acad. Sci. **125**, 235 (1897).
[2]*Physics and Applications of Invar Alloys*, edited by H. Saito (Maruzen, Tokyo, 1978).
[3]E. F. Wassermann, in *Ferromagnetic Materials*, edited by K. H. J. Buschow and E. P. Wohlfarth (Elsevier, Amsterdam, 1990), Vol. 5.
[4]G. Y. Chin, IEEE Trans. Magn. **7**, 102 (1971).
[5]K. H. Kim, B.-T. Lee, and C.-J. Choi, J. Alloys Compd. **491**, 391 (2010).
[6]P. C. Srivastava and P. S. Pandey, Solid State Commun. **150**, 1392 (2010).
[7]M. Thakur, K. De, S. Giri, S. Si, A. Kotal, and T. K. Mandal, J. Phys.: Condens. Matter **18**, 9093 (2006).
[8]S. Das, S. Majumdar, and S. Giri, J. Solid State Chem. **184**, 2215 (2011).
[9]X. Chen, S. Bedanta, O. Petracic, W. Kleemann, S. Sahoo, S. Cardoso, and P. P. Freitas, Phys. Rev. B **72**, 214436 (2005).
[10]S. Sahoo, O. Petracic, W. Kleemann, P. Nordblad, S. Cardoso, and P. P. Freitas, Phys. Rev. B **67**, 214422 (2003).
[11]S. Sahoo, O. Petracic, Ch. Binek, W. Kleemann, J. B. Sousa, S. Cardoso, and P. P. Freitas, Phys. Rev. B **65**, 134406 (2002).
[12]W. Kleemann, O. Petracic, Ch. Binek, G. N. Kakazei, Yu. G. Pogorelov, J. B. Sousa, S. Cardoso, and P. P. Freitas, Phys. Rev. B **63**, 134423 (2001).
[13]S. Bedanta and W. Kleemann, J. Phys. D: Appl. Phys. **42**, 013001 (2009).
[14]M. Thakur, M. Patra, S. Majumdar, and S. Giri, J. Appl. Phys. **105**, 073905 (2009).
[15]X. Batlle, N. Pérez, P. Guardia, O. Iglesias, A. Labarta, F. Bartolomé, L. M. García, J. Bartolomé, A. G. Roca, M. P. Morales, and C. J. Serna, J. Appl. Phys. **109**, 07B524 (2011).
[16]C. Kittel, *Introduction to Solid State Physics* (Wiley Eastern Limited, New Delhi, 1977).
[17]K. Binder and A. P. Young, Rev. Mod. Phys. **49**, 435 (1977).
[18]T. Zhang, X. G. Li, X. P. Wang, Q. F. Fang, and M. Dressel, Eur. Phys. J. B **74**, 309 (2010).
[19]M. Ulrich, J. García-Otero, J. Rivas, and A. Bunde, Phys. Rev. B **67**, 024416 (2003).
[20]F. Rivadulla, M. A. López-Quintela, and J. Rivas, Phys. Rev. Lett. **93**, 167206 (2004).
[21]K. De, S. Majumdar, and S. Giri, J. Phys. D: Appl. Phys. **40**, 5810 (2007).
[22]X. Chen, S. Sahoo, W. Kleemann, S. Cardoso, and P. P. Freitas, Phys. Rev. B **70**, 172411 (2004).
[23]M. Thakur, M. Pal Chowdhury, S. Majumdar, and S. Giri, Nanotechnology **19**, 045706 (2008).
[24]K. Jonason, E. Vincent, J. Hammann, J. P. Bouchaud, and P. Nordblad, Phys. Rev. Lett. **81**, 3243 (1998).
[25]Y. Sun, M. B. Salamon, K. Garnier, and R. S. Averback, Phys. Rev. Lett. **91**, 167206 (2003).
[26]S. Chakraverty, M. Bandyopadhyay, S. Chatterjee, S. Dattagupta, A. Frydman, S. Sengupta, and P. A. Sreeram, Phys. Rev. B **71**, 054401 (2005).
[27]M. Sasaki, P. E. Jönsson, H. Takayama, and H. Mamiya, Phys. Rev. B **71**, 104405 (2005).
[28]V. Markovich, I. Fita, A. Wisniewski, G. Jung, D. Mogilyansky, R. Puzniak, L. Titelman, and G. Gorodetsky, Phys. Rev. B **81**, 134440 (2010).
[29]M. Thakur, S. Majumdar, S. Giri, A. Bhaumik, M. Nandi, H. Nakamura, H. Kobayashi, and T. Kohara, J. Phys.: Condens. Matter **20**, 295228 (2008).
[30]M. Sasaki, P. E., Jönsson, H. Takayama, and P. Nordblad, Phys. Rev. Lett. **93**, 139701 (2004).
[31]R. K. Zheng, H. Gu, and X. X. Zhang, Phys. Rev. Lett. **93**, 139702 (2004).
[32]R. K. Zheng, H. Gu, B. Xu, and X. X. Zhang, Phys. Rev. B **72**, 014416 (2005).
[33]H. Mamiya, I. Nakatani, and T. Furubayashi, Phys. Rev. Lett. **82**, 4332 (1999).
[34]A. Bhattacharyya, S. Giri, and S. Majumdar, Phys. Rev. B **83**, 134427 (2011).
[35]D. S. Fisher and D. A. Huse, Phys. Rev. Lett. **56**, 1601 (1986).
[36]F. Lefloch, J. Hammann, M. Ocio, and E. Vincent, Europhys. Lett. **18**, 647 (1992).
[37]M. Mandal, S. Kundu, T. K. Sau, S. M. Yusuf, and T. Pal, Chem. Mater. **15**, 3710 (2003).
[38]R. Nazir, M. Mazhara, M. J. Akhtarb, M. Nadeemb, M. Siddiqueb, R. Shahc, and S. K. Hasanaind, J. Alloys Compd. **479**, 97 (2009).
[39]Y. Vasquez, A. K. Sra, and R. E. Schaak, J. Am. Chem. Soc. **127**, 12504 (2005).
[40]L. Bogani, L. Cavigli, C. de Julián Fernández, P. Mazzoldi, G. Mattei, M. Gurioli, M. Dressel, and D. Gatteschi, Adv. Mater. **22**, 4054 (2010).